Polarization and Transverse Mode Dynamics of Gain-Guided Vertical-Cavity Surface Emitting Lasers

J. Martín-Regalado, S. Balle, M. San Miguel

Instituto Mediterraneo de Estudios Avanzados, IMEDEA (CSIC-UIB) and
Departament de Física, Universitat de les Illes Balears (UIB), E-07071 Palma de Mallorca, Spain. E-mail: josep@hp1.uib.es

Transverse mode competition and polarization selection in gain-guided Vertical Cavity Surface Emitting Lasers are studied using a transverse continuous model which incorporates basic physical mechanisms of polarization dynamics. Polarization stability and polarization switching within the fundamental Gaussian mode are described. The first order transverse mode always starts lasing orthogonally polarized to the fundamental one. At larger currents polarization coexistence with several active transverse modes occur. These results are shown to be sensitive to the carrier spin-flip relaxation rate.

A practical limitation of many Vertical Cavity Surface Emitting Lasers (VCSELs) is the polarization and transverse mode instabilities which appear as the injected current is increased beyond the threshold value [1]. Narrow contact VCSELs tend to operate in the fundamental TEM_{00} mode for any current value. Although stable polarization emission is observed in some VCSELs [2], changes in the polarization state of the TEM_{00} mode (polarization switching) are often observed as the injection current is raised [3]. In wider contact VCSELs, TEM_{00} mode emission is restricted to a current range close above the lasing threshold. For larger currents, higher order transverse modes come into play. It is generally observed that when the first order transverse mode starts lasing it is orthogonally polarized to the TEM_{00} mode [4–8]. In the injection range of TEM_{00} emission there can be either stable polarization emission [4–6] or polarization switching [6–8], thus defining two general scenarios. The mechanisms of transverse mode competition mediated by polarization dynamics are not well understood. In this letter we account for the generally observed scenarios by incorporating transverse degrees of freedom in a model previously used to successfully describe the polarization dynamics of the fundamental transverse mode in narrow contact VCSELs [9].

The model we use is based on the coupling of the circularly polarized components of the vector electric field ($E_\pm$) to the different spin sublevels of the conduction and the heavy-hole valence bands in quantum well VCSELs [10]. In order to describe gain-guided (proton implanted) VCSELs we use a continuous transverse *(x,y)* description of the optical field and the medium variables by considering optical field diffraction and carrier diffusion. We also incorporate dynamical equations for the material polarization which provide a frequency-dependent gain and dispersion since we need to describe mode competition between transverse modes separated around 100 GHz in frequency. The equations describing the spatio-temporal and polarization properties of a single-longitudinal mode gain-guided VCSEL thus become

$$\begin{aligned}
\partial_t E_\pm(x,y;t) &= -\kappa(1-i\alpha)E_\pm + P_\pm + \\
&+ i\frac{c^2}{2\Omega\, {n_e}^2}\nabla_\perp^2 E_\pm - \\
&- (\gamma_a + i\gamma_p)E_\mp \ , && (1)\\
\partial_t P_\pm(x,y;t) &= -\gamma_\perp(1+i\alpha)P_\pm + \\
&+ \gamma_\perp a(N \pm n - N_0)E_\pm + \\
&+ \sqrt{\beta(N\pm n)}\chi_\pm(x,y;t) \ , && (2)\\
\partial_t N(x,y;t) &= C(x,y) - \gamma_e N + D\nabla_\perp^2 N - \\
&- \left[(E_+P_+^* + E_-P_-^*) + c.c.\right] , && (3)\\
\partial_t n(x,y;t) &= -\gamma_s n + D\nabla_\perp^2 n - \\
&- \left[(E_+P_+^* - E_-P_-^*) + c.c.\right] , && (4)
\end{aligned}$$

where $P_\pm$ are the associated nonlinear material polarizations in a two-level Maxwell-Bloch approximation (a discussion of this approximation for semiconductor lasers is given in [11]), $N - N_0$ is the total carrier distribution referred to transparency (N_0), and n is the difference of the carrier distributions associated with E_+ and E_-. Diffraction is taken into account in a longitudinal mean field approximation by the transverse laplacian term in Eqs. (1). In our gain-guided situation diffraction leads to the selection of transverse mode profiles and associated frequencies [11]. The decay rates used are κ ($300\ ns^{-1}$), $\gamma_\perp$ ($20\ ps^{-1}$) which gives a measure of the gain bandwidth, γ_e ($1\ ns^{-1}$), and γ_s ($50\ ns^{-1}$) which takes into account the spin-flip relaxation processes that couple the emission channels [9,10]. Other parameters in Eqs. (1)–(4) are the α-factor (3), the carrier frequency Ω corresponding to the emission wavelength λ ($750\ nm$), the refractive index n_e (3.55), the differential gain a ($10^{-6}\mu m^3 ps^{-1}$), and the carrier diffusion constant D ($3\ cm^2/s$). Material anisotropies are introduced through the last term in Eq. (1). The birefringence, γ_p, splits the emission frequency of the linearly polarized fields [12], given by $E_x = (E_+ + E_-)/\sqrt{2}$ and $E_y = -i(E_+ - E_-)/\sqrt{2}$, whereas the dichroism, γ_a, accounts for their different gain-to-loss ratio due to anisotropies in the cavity geometry. The total injected current, I, is assumed to be uniformly distributed across a circular region of diameter ϕ (VCSEL contact) defining the transverse current density distribution, $C(x, y)$. Spontaneous emission processes are modeled by a noise source $\chi_{\pm}$ [11]. The total CW output power obtained from Eqs. (1)–(4) is essentially independent of the parameters specific to polarization dynamics.

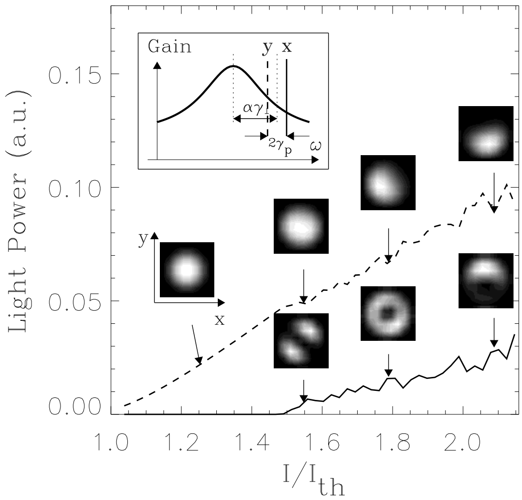

FIG. 1. *L-I characteristic for the linearly $\hat{x}$ (solid) and $\hat{y}$ (dashed) polarizations for ϕ=12.5 μm, γ_p=3γ_e and γ_a=0. Assuming a quantum efficiency of 100 %, a 1.5 μm cavity length and a QW thickness of 80 nm, with our parameters we have that for this VCSEL each unit in the y-axis corresponds to $\approx$ 14 mW of output power. Instantaneous transverse near-field profiles are shown at the indicated points. The plotted area corresponds to a square of* $10x10\mu m^2$ *and the width of the* TEM_{00} *mode is about* 60% *of the current contact. The inset shows the Maxwell-Bloch two-level gain spectrum and the location of the linearly polarized* TEM_{00} *modes for the set of parameters chosen. The gain difference between the two orthogonally polarized modes is* $0.053\gamma_e$.

The results presented here have been obtained by numerical integration of the model equations for circular contact VCSELs with a fixed birefringence, different diameters and slightly different dichroism values. The first VCSEL we study has a diameter $\phi = 12.5$ μm, $\gamma_p = 3\gamma_e$ and $\gamma_a = 0$, with a threshold current of $I_{th} \sim 5mA$. For this device, the selection of the polarization direction at threshold comes as a consequence of birefringence which provides slightly different material gain coefficients for the two linearly polarized fields (see the inset in Fig. 1). For the chosen sign of γ_p, the VCSEL starts lasing close to threshold (at $I = 1.05I_{th}$) with a $\hat{y}$–TEM_{00} mode. Fig. 1 shows the polarized L-I characteristics for this device obtained by increasing the current applied to the device continuously in time from $I = 1.05I_{th}$ to $I = 2.16I_{th}$. The output power emitted by the VCSEL increases linearly with the current and stable $\hat{y}$–polarized fundamental mode emission is observed up to $I \sim 1.50I_{th}$. For larger current values higher order modes start lasing in both polarizations. In the multitransverse mode regime, the $\hat{y}$–polarized beam profile consists on a single lobe with the peak moving around the VCSEL contact as the current increases. On the other hand, although the $\hat{x}$–polarized beam profile can adopt a doughnut-shape (see e.g. at $I \sim 1.79I_{th}$) or a single, not-centered lobe distribution (see e.g. at $I \sim 2.08I_{th}$), it often consists on two lobes oscillating in time around the center of the VCSEL. Such L-I characteristic corresponds to the scenario observed in some VCSELs. [4–6]

Fig. 2 shows the L-I characteristics for a VCSEL with $\phi = 10$ μm, $\gamma_p = 3\gamma_e$ and $\gamma_a = -5\gamma_e$ ($I_{th} \sim 3mA$). For this narrower device, the current range where the TEM_{00} mode dominates is larger than in the previous VCSEL. In addition, as compared to the previous case we have now introduced a loss anisotropy, γ_a, in such a way that, although the material gain for $\hat{y}$-polarized fields is higher than for $\hat{x}$-polarization, the net gain for $\hat{x}$–polarized fields is higher than that for $\hat{y}$–polarized fields. As a consequence the VCSEL emits at threshold an $\hat{x}$–TEM_{00} mode whereas the $\hat{y}$–polarization is off. However, around $I \sim 1.45I_{th}$, polarization switching occurs without changing the transverse beam profile as a consequence of phase dynamics, as described in [9]. For currents values beyond the switching current the $\hat{y}$–polarization retains the Gaussian shape of the TEM_{00} mode. At $I \sim 1.85I_{th}$ an $\hat{x}$–polarized first order transverse mode appear. Beyond this current value, the $\hat{x}$–polarized total power increases almost linearly while $\hat{y}$–polarized total power saturates. Such general behavior corresponds to the scenario found in [6–8].

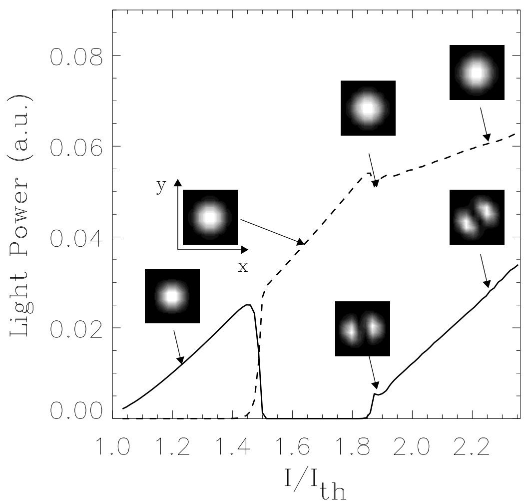

FIG. 2. *Same as in Fig. 2 but for ϕ=10 μm, γ_p=3γ_e and γ_a=-5γ_e, which favors $\hat{x}$-polarization at threshold. Now, each unit in the vertical axis corresponds to $\approx$ 9 mW.*

The modal behavior of the VCSEL emission is described in Fig. 3 where we show the optical spectra and the transverse mode profiles at four current values indicated with arrows in Fig. 2. These spectra are equivalent to those obtained by a Fabry-Perot interferometer with a FSR of 1 THz and a frequency resolution of 1 GHz. At $I \sim 1.29I_{th}$ (see Fig. 3(a)) the laser emits in the $\hat{x}$–TEM_{00} mode although the off–polarization shows an amplified spontaneous emission peak [4]. Beyond the switching point, at $I \sim 1.67I_{th}$, laser emission now occurs in the $\hat{y}$–TEM_{00} mode (Fig. 3(b)). At $I \sim 1.87I_{th}$ there is coexistence of both polarizations with different transverse profiles: a $\hat{y}$–TEM_{00} mode (α) and a $\hat{x}$–TEM_{10} mode (β). Finally, Fig. 3(d) shows the spectrum at $I \sim 2.26I_{th}$. The TEM_{00} mode (α)

dominates $\hat{y}$–polarized emission although several second order modes (δ and ϵ) appear with 40 dB of mode suppression. In the $\hat{x}$–polarization, two frequency nondegenerate first-order modes, the TEM_{10} (β) and the TEM_{01} (γ) modes are clearly distinguishable in the optical spectrum as described in [12]. At this current, the $\hat{x}$–polarized beam profile consists on two-lobes which oscillate periodically around the center of the VCSEL, the frequency of the oscillation given by the beat note of the first-order transverse modes. For larger current values (not shown in the figure) several transverse modes are excited and there is coexistence of both polarizations in every transverse mode.

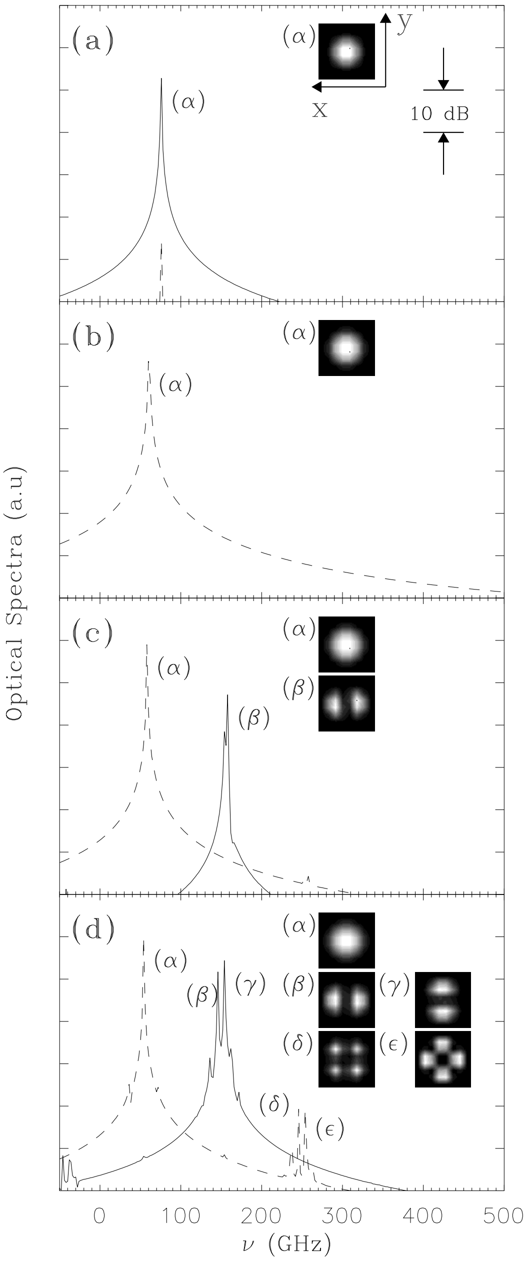

FIG. 3. *Optical spectra of the linearly polarized field components E_x (solid) and E_y (dashed) for fixed current values indicated in Fig. 2 by arrows: (a) $I = 1.29 I_{th}$, (b) $I = 1.67 I_{th}$, (c) $I = 1.87 I_{th}$, (d) $I = 2.26 I_{th}$. The insets show the spatially resolved near-field patterns at the labeled peaks (transverse modes).*

We have also studied the case of very fast spin-flip relaxation ($\gamma_s = 500\gamma_e$). In this case we find that the transverse dynamics is not sensitive to polarization: the VCSEL of Fig. 2 emits $\hat{x}$–polarized light at any current value, even in the multitransverse mode regime, which now is postponed to $I \sim 2.2 I_{th}$. From this result we infer that physical mechanisms associated with γ_s are crucial to describe the observed emergence of higher order transverse modes orthogonally polarized to the TEM_{00} mode.

In summary, we have shown that commonly observed scenarios of transverse mode competition and polarization selection in gain-guided VCSELs can be accounted for by a model which incorporates the vector nature of the laser field, optical field diffraction, carrier diffusion, and the basic physical mechanisms of polarization dynamics.

The authors wish to thank Prof. N.B. Abraham for helpful discussions and comments. We acknowledge financial support from CICYT (Spain) projects TIC95/0563 and PB94-1167, and European Union TMR Grant QSTRUCT FMRX-CT96-0077.

---

[1] C.J. Chang-Hasnain, J.P. Harbison, G. Hasain, A.C. Von Lehmen, L.T. Florez and N.G. Stoffel, IEEE J. Quantum Electron. **27**, 1402 (1991); H. Li, T.L. Lucas, J.G. McInerney and R.A. Morgan, Chaos, Solitons and Fractals **4**, 1619 (1994).

[2] F. Koyama, K. Morito, and K. Iga, IEEE J. Quantum Electron. **27**, 1410 (1991).

[3] Z.G. Pan, S. Jiang and M. Dagenais, R.A. Morgan, K. Kojima, M.T. Asom, R.E. Leibenguth, G.D. Guth, and M.W. Focht, Appl. Phys. Lett. **63**, 2999 (1993).

[4] M.P. van Exter, A.K. Jansen van Doorn, R.F.M. Hendriks, and J.P. Woerdman, Proc. SPIE **2693**, 202 (1996).

[5] K.D. Choquette, R.P. Schneider Jr., K.L. Lear, and R.E. Leibenguth, IEEE J. of Sel. Topics in Quantum Electron. **1**, 661 (1995).

[6] J.H. Ser, Y.G. Ju, J.H. Shin, and Y.H. Lee, Appl. Phys. Lett. **66**, 2769 (1995).

[7] K.D. Choquette, D.A. Richie, and R.E. Leibenguth, Appl. Phys. Lett. **64**, 2062 (1994).

[8] U. Fiedler, G. Reiner, P. Schnitzer, and K.J. Ebeling, IEEE Phot. Tech. Lett. **8**, 746 (1996).

[9] J. Martín-Regalado, M. San Miguel, N.B. Abraham and F. Prati, *Opt. Lett.* **21**, 351 (1996); J. Martín-Regalado, F Prati, M. San Miguel and N.B. Abraham, Proc. SPIE **2693**, 213 (1996), and *submitted to IEEE J. Quantum Electronics.*

[10] M. San Miguel, Q. Feng, J.V. Moloney, Phys. Rev. A **52**, 1728 (1995).

[11] J. Martín-Regalado,, G.H.M. van Tartwijk, S. Balle, and M. San Miguel, Phys. Rev. A **54**, 5386 (1996).

[12] A.K. Jansen van Doorn, M.P. van Exter and J.P. Woerdman, Electron. Lett. **30**, 1941 (1994).